RSC Advances

ROYAL SOCIETY OF CHEMISTRY

www.rsc.org/advances

Electronic and Electrochemical Properties as well as Flowerlike Supramolecular Assemblies of Fulleropyrrolidines Bearing Ester Substituent with Different Alkyl Chain Length

Xuan Zhang*, Xu-Dong Li, Li-Xia Ma, Bei Zhang

College of Chemistry, Chemical Engineering & Biotechnology, Donghua University, Shanghai 201620, China.

Corresponding Author: xzhang@dhu.edu.cn

Abstract:

A series of alkyl (methyl, ethyl, propyl, butyl) benzoate ester substituted fulleropyrrolidine derivatives (**FP1**–**FP4**) were synthesized and their electronic and electrochemical properties were investigated by means of absorption spectra, electronic structure calculation, and cyclic voltammetry (CV), respectively. The LUMO/HOMO energies and energy gaps of fullerene derivatives were estimated by the first reduction potential measured with CV combined with absorption spectra, which are in consistent with those obtained from density functional theory (DFT) calculations. It was found that all fulleropyrrolidines showed the very similar absorption spectra, orbital energies and redox behaviors, which are comparable with those of well-known phenyl-C_{61}-butyric acid methyl ester (PCBM). The flowerlike supramolcular architectures obtained from self-assembly of **FP1**–**FP4** in chloroform/alcohol mixture solvents were characterized by scanning electron microscopy (SEM) and X-ray diffraction (XRD). A lamellar structure with a d-spacing of 1.92–2.02 nm that depends on their molecular sizes, corresponding to the thickness of a bilayer structure, suggested a face-to-face conformation of the substituent of C_{60} and an interdigitation of the bare C_{60} side packing fashion. These fulleropyrrolidines are high C_{60} content, energetically PCBM-like, and capable of forming complex flowerlike architectures, which provide fundamental insights into molecular design toward advanced fullerene materials.

Keywords:

Fullerenes, Electronic calculation, Electrochemistry, Flowerlike assemblies, Lamellar structure

1. Introduction

Fullerene (C_{60}) and its derivatives have considerably been employed as an excellent electron-acceptor material in various optoelectronic devices (such as organic solar cells and field effect transistors).[1–6] On the other hand, as typical π-conjugated molecules, fullerenes are also important building blocks for fabrication of functional supramolecular assemblies.[7–10] It has been recognized that the performance of molecular device could be improved by fine molecular-tailoring and directed self-organization of π-conjugated units. In this regard, many efforts have been devoted to self-assembly of fullerenes to manipulating properties of fullerene-based materials.[11–19] For example, several well-defined organized nano/microstructures such as spheres,[20] rods,[21] wires,[22] belts,[23,24] whiskers,[25,26] and sheets,[27,28] have been fabricated from the pristine C_{60}, which retain the intrinsic optoelectronic properties of fullerenes but the numbers of solvents owning enough solubility for C_{60} are very limited (usually aromatic solvents and carbon disulfide). Alternatively, molecular-tailoring of fullerenes via attachment of proper substituent groups on periphery of C_{60} cage not only enhances its solubility in common organic solvents, which is benefit for solution processing in device fabrication, but also enables the regulation of self-assembly.[29–44] For example, various superstructures such as nanofibers, vesicles, flowerlike architectures have been achieved by fulleropyrrolidines bearing multiple alkyl chains.[41–44] However, the attachment of bulky and insulating appends largely decreased C_{60} content (usually lower than 50%), leading to these chemically-modified fullerenes are less electronically active that is actually undesirable for their optoelectronic applications. Therefore, grafting small substituent groups on fullerene surface should be more promising due to high C_{60} content will be retained in these fullerene derivatives.[45,46] Recently, a small pyridine group equipped fulleropyrrolidine was reported to be capable of organizing into C_{60}-rich and photoconductive flowerlike architectures, which retain high C_{60} content (84%) and photoinduced carrier-transporting properties comparable with pristine C_{60}.[45] Furthermore, it was also found that the morphology of self-organized objects could also be tuned by the position of N-atom in pyridine group. This example provides a useful molecular design concept for construction of C_{60}-rich complex supramolecular assemblies via grafting a small substituent group on periphery of fullerene cage. Thus the design and synthesis of other small substituent attached fullerene derivatives to investigate their electronic properties and self-assembly would further provide fundamental insights into fullerene-containing materials.

In this work, by considering the molecular structure of well-known fullerene derivative, phenyl-C61-butyric acid methyl ester (PCBM), a small benzoate ester substituent group was then grafted on C_{60} to synthesize a series of alkyl (methyl, ethyl, propyl, butyl) benzoate ester-substituted fulleropyrrolidines (**FP1**–**FP4**, Scheme 1), and their electronic and electrochemical properties as well as self-assembly were investigated by means of absorption spectra, electronic structure calculation, cyclic voltammetry (CV), scanning electron microscopy (SEM) and X-ray diffraction (XRD) analysis, respectively. It was found that the LUMO/HOMO levels of these fullerene derivatives estimated by the experiments and theoretical calculations, are energetically PCBM-like. All of these fulleropyrrolidines could organize into flowerlike architectures of lamellar structures with alkyl chain length dependent d-spacing. These small ester substituent attached fullerenes are high C_{60} content (76-79%), energetically PCBM-like, and capable of forming flowerlike assemblies, which provide fundamental insights into molecular design toward advanced fullerene materials.

2. Experimental details

Absorption, ^{1}H NMR and mass spectra were recorded on a TU-1901 (Persee), Brucker Avance III (400 MHz) and MALDI-TOF-MS (AB Sciex 4700) spectrometer, respectively. Scanning electron microscopy (SEM) and transmission electron microscopy (TEM) were performed on a HITACHI TM-1000 and JEOL-2100 microscopes, respectively. X-ray diffraction (XRD) patterns were obtained using a RIGAKU D/Max-2550 PC X-ray diffractometer. Cyclic voltammetry (CV) and differential pulse voltammetry (DPV) curves were measured using a CHI 660D electrochemical workstation (Chenhua, Shanghai). The CV and DPV curves were collected at room temperature under N_2 using a conventional three-electrode system (glassy carbon working electrode, Pt wire counter-electrode and Ag/Ag^+ quasi-reference electrode) in 0.1 M tetrabutylammonium Tetrafluoroborate (n-Bu_4BF_4) solution in 1,2-dichlorobenzene (o-DCB) at a potential scan rate of 100 mV/s, where the reduction potentials were calibrated using ferrocene/ferrocenium (Fc/Fc^+) redox couple as internal standard. The geometries of fulleropyrrolidine derivatives were optimized by density functional theory (DFT) at the B3LYP/6-31G(d) level, and the orbital energy and orbital analysis were calculated at the PBEPBE/6-311G(d,p) level, with the Gaussian 09 program package.[47]

Fullerene C_{60} (99%) was purchased from XFNANO (Nanjing) and other reagents as well as solvents (AR) were obtained from Sinopharm Chemical Reagents Co. (Shanghai). Alkyl (methyl, ethyl, propyl, butyl) 4-formylbenzoates were prepared by esterification reaction from 4-formylbenzoic acid with the corresponding alcohols in the presence of thionyl chloride. Fulleropyrrolidine derivatives (**FP1**–**FP4**, Scheme 1) were synthesized by refluxing the toluene solution of C_{60}, sarcosine and the corresponding benzaldehyde according to the standard Prato reaction.[48]

1, ^{1}H NMR (400 MHz, $CDCl_3$): δ (ppm) = 8.12 (d, 2H, J = 8.0 Hz), 7.94 (br, 2H), 5.07 (br, 2H), 4.33 (d, 1H, J = 8.0 Hz), 3.91 (s, 3H), 2.85 (s, 3H). MALDI-TOF-MS [DCTB] m/z calcd., $C_{71}H_{13}NO_2$ 911.23; found, 911.12.

2, ^{1}H NMR (400 MHz, $CDCl_3$): δ (ppm) = 8.13 (d, 2H, J = 8.0 Hz), 7.96 (br, 2H), 5.11 (br, 2H), 4.40-4.35 (m, 3H), 2.88 (s, 3H), 1.39 (t, 3H, J = 8.0 Hz). MALDI-TOF-MS [DCTB] m/z calcd., $C_{72}H_{15}NO_2$ 925.25; found, 925.76.

3, ^{1}H NMR (400 MHz, $CDCl_3$): δ (ppm) = 8.12 (d, 2H, J = 8.0 Hz), 7.92 (br, 2H), 5.05 (br, 2H), 4.33-4.25 (m, 3H), 2.84 (s, 3H), 1.82-1.76 (m, 2H), 1.03 (t, 3H, J = 8.0 Hz). MALDI-TOF-MS [DCTB] m/z calcd., $C_{73}H_{17}NO_2$ 939.28; found, 939.86.

4, ^{1}H NMR (400 MHz, $CDCl_3$): δ (ppm) = 8.13 (d, 2H, J = 8.0 Hz), 7.97 (br, 2H), 5.12 (br, 2H), 4.37-4.30 (m, 3H), 2.88 (s, 3H), 1.79-1.71 (m, 2H), 1.51-1.45 (m, 2H), 0.98 (t, 3H, J = 8.0 Hz). MALDI-TOF-MS [DCTB] m/z calcd., $C_{74}H_{19}NO_2$ 953.31; found, 953.87.

3. Results and discussion

3.1. Photophysical properties.

The absorption spectra (400–750 nm) of fulleropyrrolidine derivatives **FP1**–**FP4** in chloroform (1.3×10^{-4} M) were shown in Figure 1, together with the spectrum of pristine C_{60} (6.5×10^{-5} M) for comparison. All of fulleropyrrolidine derivatives exhibit nearly the same broad absorption bands from 400 to 750 nm those extend to longer wavelength range than that of the pristine C_{60} (Figure 1). The difference of photophysical properties between **FP1**–**FP4** and the pristine C_{60} could be explained from the symmetry breaking effect in the former that enhanced the forbidden transitions to some extent.[49] It was noted that the fulleropyrrolidine derivatives

have stronger visible light absorption in the red-shifted absorption edge above 650 nm with the longer λ_{onset} around 724 nm (Table 1), which is similar to that of PCBM and important to contribute the light harvesting in photovoltaics.[46] The similar absorption spectra observed among fulleropyrrolidine derivatives **FP1**–**FP4** indicated that the alkyl chain length scarcely affects their photophysical properties.

3.2. Electrochemical properties.

It is well-known that fullerenes have rich electrochemical property and can accept up to six electrons in solution.[50,51] The first reduction potentials of fullerene acceptors were usually used to estimate their lowest unoccupied molecular orbital (LUMO) energy, which determines the open circuit voltage performance of polymer solar cells together with the highest occupied molecular orbital (HOMO) energy levels of electron donor.[52–54] We therefore measured the cyclic voltammograms of **FP1**–**FP4** and the pristine C_{60} for a comparison. As shown in Figure 2, a series of cyclic voltammograms shows that three well-defined and reversible redox waves are retained in the functionalized fullerenes ranging from 0 to –2.6 V vs Ag/Ag^+, under room temperature and anhydrous air-free conditions, relative to the ferrocene/ferrocenium (Fc/Fc^+) internal standard. As shown in Figure 3, three sharp and equal intensity peaks together with the noticeable fourth peaks were clearly observed from differential pulse voltammetry (DPV), further revealing that **FP1**–**FP4** are typical redox-reversible fullerene derivatives. From the CV, it can be noted that three reversible redox peaks of all derivatives **FP1**–**FP4** are all shifted to negative potentials by ca. 100 mV as compared to those of C_{60}, an indication of the stronger electron acceptor. The measured half-wave potentials are listed in Table 1 together with the LUMO energy levels of the fullerene derivatives, estimated from the their onset reduction potentials (E_{onset}^{red}) according to the equation, LUMO (eV) = − e (E_{onset}^{red} + 4.60).[55] The E_{onset}^{red} of **FP1**–**FP4** were −0.77, −0.78, −0.78, and −0.78 V, corresponding to the LUMO energy levels of −3.83, −3.82, −3.82, and −3.82 eV, respectively (Table 1), indicating the alkyl chain length has a little effect on their electrochemical properties. The LUMO energy levels of **FP1**–**FP4** are ca. 0.1 eV higher than that of C_{60} (−3.92 eV), which is desirable for an electron acceptor in polymer solar cells to get higher open-circuit voltage.[52–54] The redox properties, LUMO, HOMO and energy gap (E_{gap}) of all derivatives are similar and also very close to those of PCBM (Table 1),[55] an indicative of **FP1**–**FP4** are PCBM-like electron acceptors.

3.3. DFT calculations.

To further understand the substituent effect on the LUMO/HOMO energy levels of fullerene acceptors, DFT calculations were performed by using the Gaussian 09 program package.[47] Ground state geometrical structures of four fulleropyrrolidine derivatives **FP1**–**FP4**, PCBM and C_{60} were optimized at the B3LYP/6-31G(d) level, and the molecular orbital energies were calculated at the more reliable PBEPBE/6-311G(d,p) level based on above optimized geometries.[49,56,57] The calculated results are summarized in Table 1, and the schematic diagrams of HOMO and LUMO levels are shown in Figure 4. It can be noted that the HOMO–LUMO energy gaps of fulleropyrrolidine derivatives **FP1**–**FP4** reduced to 1.72 eV by comparison with 1.79 eV of C_{60}, while their LUMO and HOMO energies are 0.17 and 0.35 eV higher than those of C_{60} (−4.18 and −5.87 eV), respectively (Figure 4 and Table 1), which may explain the red-shifted absorption of substituted fullerenes. The calculated orbital energies of derivatives **FP1**–**FP4** are nearly same as those of PCBM and also close to the experimental values (Table 1), confirming the PBE method a reliable in orbital energy calculation for fullerene systems. In addition, other molecular properties, such as molecular hardness, electrophilicity, electronegativity, etc., have also been provided (Table S2, ESI†). Considering the molecular hardness, large value means a hard molecule with less global reactivity. It was noted that the fulleropyrrolidine derivatives **FP1**–**FP4** have smaller hardness values (ca. 0.75 eV) than that of C_{60} (ca. 0.84 eV), revealing they are more reactive. Orbital analysis of HOMO and LUMO were also carried out for **FP1**–**FP4**, PCBM and C_{60} at the PBEPBE/6-311G(d,p) level (Figure 5). The fulleropyrrolidine derivatives **FP1**–**FP4**, PCBM and C_{60} showed very similar orbital distributions, in which both the LUMO and HOMO are mainly located on the fullerene cage, respectively. But it can still be noted that the electron delocalization for fullerene derivatives are slightly weakened relative to C_{60}, which has been attributed to symmetry breaking of C_{60} molecule by functionalization.[49,56] It should be noted that C_{60} has 3-fold degenerated LUMOs and 5-fold degenerated HOMOs (Fig. S1, ESI†), but the LUMO and HOMO of fulleropyrrolidine derivatives **FP1**–**FP4** become non-degenerated (Table S3 and Fig. S2, ESI†). Further orbital analysis for other occupied and vacant MOs showed that the highest occupied and lowest vacant MOs localized on phenyl substituent are energetically far from the HOMO and LUMO of **FP1**–**FP4** (Figs. S3-S6 and Table S3, ESI†), suggesting a little contribution to the frontier MOs. These findings suggest that the hybridization change (from sp^2 to sp^3) of C_{60} carbon atoms

involved in connection with substituent, which modified the localization and the nature of HOMO and LUMO, also contribute to the observed substituent effect. The similar orbital distribution of fullerene derivatives may explain the similar electronic and electrochemical properties observed in absorption spectra and CV.

3.4. Self-assembly.

To demonstrate how the small alkyl benzoate ester substituent groups affect the packing of C_{60} molecules in solid state, the self-organized objects of **FP1**–**FP4** were further investigated by SEM, TEM and XRD. The self-organized objects were prepared by mixing the chloroform solution of **FP1**–**FP4** (1 mg/ml) with 2-propanol or ethanol (10:1, v/v), then dropping on Si wafers and evaporating the solvent in a capped petri dish up to 1 h until dryness at room temperature. The assembled objects on Si wafers were directly used for SEM or XRD characterization, while they were scratched off and dispersed in EtOH for a TEM. Figure 6 shows SEM and TEM images of self-organized architectures formed from **FP1**–**FP4** derivatives. It can be noted that flowerlike objects with size distribution around 2–8 μm were consisted of plate nanostructures (Figure 6a–e), which was also confirmed by TEM (Figure 6f). To get information on molecular packing, the bulk flowerlike objects obtained from **FP1**–**FP4** on Si wafer were further investigated by XRD (Figure 7). As shown in Figure 7, one intense diffraction peak appeared at around 5° accompanied by several weaker peaks at higher angle region in **FP1**–**FP4** derivatives, resembling those previously observed in others fulleropyrrolidines.[42–46,58] These peaks are therefore similarly attributed to the reflections of (001), (002) and (003) planes with a d spacing value of 1.92, 1.95, 1.98 and 2.02 nm for **FP1**, **FP2**, **FP3**, and **FP4**, respectively, suggesting a lamellar structure. In addition, by comparison with the patterns obtained from the pristine C_{60}, the residue peaks can be readily assigned to the reflections of (111), (220), (311) and (222) planes of a fcc structure with the average spacing of 0.8 nm (as indicated by asterisks in Figure 7), suggesting a π–π (C_{60}/C_{60}) interaction in the assemblies. By taking the molecular size of 1.3–1.5 nm of **FP1**–**FP4** obtained from the DFT calculation, the d-spacing of 1.92–2.02 nm that depends their molecular sizes, corresponds well to the thickness of a bilayer structure, where a face-to-face conformation of the substituent of C_{60} and an interdigitation of the bare C_{60} side packed as suggested before.[7,13,45,58] These observations suggest that the smaller grafted group insufficiently

disturbing the strong π–π interactions between adjacent C_{60} molecules,[13] especially the strongest peaks from fcc packing were clearly noticed in the case of **FP1** (Figure 7).

4. Conclusions

In conclusion, a series of small alkyl (methyl, ethyl, propyl, butyl) benzoate ester group substituted fulleropyrrolidine derivatives (**FP1**–**FP4**) were synthesized and their electronic and electrochemical properties as well as self-assembly were investigated by means of absorption spectra, DFT calculation, CV, SEM, TEM and XRD, respectively. The LUMO/HOMO energies of fullerene derivatives were estimated by the first reduction potential measured with CV combined with absorption spectra, which are in consistent with those obtained from DFT calculations. All fulleropyrrolidines **FP1**–**FP4** showed the very similar absorption spectra, orbital energies and redox behaviors, which are comparable with those of well-known PCBM, indicating alkyl chain length has little effect on their electronic and electrochemical properties. The SEM investigation of self-assembly of **FP1**–**FP4** in chloroform/alcohol solution mixture solvents showed that flowerlike supramolcular architectures can be facilely achieved. XRD analysis revealed that these flowerlike objects were lamellar structures with the d-spacing of 1.92–2.02 nm that depends on the molecular size of **FP1**–**FP4**, corresponding well to the thickness of a bilayer structure. This suggested a face-to-face conformation of the substituent of C_{60} and an interdigitation of the bare C_{60} side packing fashion. The fulleropyrrolidines **FP1**–**FP4** are high C_{60} content (76–79%), energetically PCBM-like, and capable of forming complex flowerlike architectures, which provide fundamental insights into molecular design toward advanced fullerene materials and may find potential application in optoelectronics.

Acknowledgements

This work was financially supported by Innovation Program of Shanghai Municipal Education Commission (12ZZ067), Shanghai Pujiang Program (11PJ1400200), the Research Fund for the Doctoral Program of Higher Education of China (20120075120018), and the Fundamental Research Funds for the Central Universities.

† Electronic supplementary information (ESI) available: Data of additional computation results for C_{60} and PCBM at various basis sets, other molecular properties (ionization potential, electro affinity, electronegativity, global hardness, etc.) and MOs for fullerenes are available.

Notes and references

1. C. Yang, J. Y. Kim, S. Cho, J. K. Lee, A. J. Heeger and F. Wudl. *J. Am. Chem. Soc.* 2008, **130**, 6444−6450.

2. J. L. Segura, N. Martín and D. M. Guldi. *Chem. Soc. Rev.* 2005, **34**, 31–47.

3. D. M. Guldi, B. M. Illescas, C. M. Atienza, M. Wielopolskia and N. Martín. *Chem. Soc. Rev.* 2009, **38**, 1587–1597.

4. C.-Z. Li, H. L. Yip and A. K. Y. Jen. *J. Mater. Chem.* 2012, **22**, 4161−4177.

5. Y. J. He and Y. F. Li. *Phys. Chem. Chem. Phys.* 2011, **13**, 1970−1983.

6. Y.-Y. Lai, Y.-J. Cheng and C. S. Hsu. *Energy Environ. Sci.* 2014, **7**, 1866–1883.

7. M. J. Hollamby, M. Karny, P. H. H. Bomans, N. A. J. M. Sommerdjik, A. Saeki, S. Seki, H. Minamikawa, I. Grillo, B. R. Pauw, P. Brown, J. Eastoe, H. Möhwald and T. Nakanishi. *Nature Chem.* 2014, **6**, 690–696.

8. H.-G. Li, J. Choi and T. Nakanishi. *Langmuir* 2013, **29**, 5394–5406.

9. Y. Yamamoto, G. Zhang, W. Jin, T. Fukushima, N. Ishii, A. Saeki, S. Seki, S. Tagawa, T. Minari, K. Tsukagoshi and T. Aida. *Proc. Natl. Acad. Sci. USA* 2009, **106**, 21051–21056.

10. V. Georgakilas, F. Pellarini, M. Prato, D. M. Guldi, M. Melle-Franco and F. Zerbetto. *Proc. Natl. Acad. Sci. USA* 2002, **99**, 5075–5080.

11. L. Sánchez, R. Otero, J. María Gallego, R. Miranda and N. Martín. *Chem. Rev.* 2009, **109**, 2081–2091.

12. T. Nakanishi. *Chem. Commun.* 2010, **46**, 3425–3436.

13 H.-G. Li, S. S. Babu, S. T. Turner, D. Neher, M. J. Hollamby, T. Seki, S. Yagai, Y. Deguchi, H. Möhwald and T. Nakanishi. *J. Mater. Chem. C* 2013, **1**, 1943–1951.

14. H. Asanuma, H.-G. Li, T. Nakanishi and H. Möhwald. *Chem. Eur. J.* 2010, **16**, 9330–9338.

15. P. Heremans, D. Cheyns and B. P. Rand. *Acc. Chem. Res.* 2009, **42**, 1740–1747.

16. A. J. Moulé and K. Meerholz. *Adv. Funct. Mater.* 2009, **19**, 3028–3036.

17. L. K. Shrestha, Q. M. Ji, T. Mori, K. Miyazawa, Y. Yamauchi, J. P. Hill and K. Ariga. *Chem. Asian J.* 2013, **8**, 1662–1679.

18. S. S. Babu, H. Möhwald and T. Nakanishi. *Chem. Soc. Rev.* 2010, **39**, 4021–4035.

19. Y.-F. Shen and T. Nakanishi. *Phys. Chem. Chem. Phys.* 2014, **16**, 7199–7204.

20. X. Zhang and M. Takeuchi. *Angew. Chem. Int. Ed.* 2009, **48**, 9646–9651.

21. L. Wang, B. Liu, D. Liu, M. Yao, Y. Hou, S. Yu, T. Cui, D. Li, G. Zou, A. Iwasiewicz and B. Sundqvist. *Adv. Mater.* 2006, 18, 1883–1886.

22. J. Geng, W. Zhou, P. Skelton, W. Yue, I. A. Kinloch, A. H. Windle and B. F. G. Johnson. *J. Am. Chem. Soc.* 2008, **130**, 2527–2534.

23. X. Zhang and X. D. Li. *Chin. Chem. Lett.* 2014, **25**, 912–914.

24. L. Wei, J. Yao and H. Fu. *ACS Nano* 2013, **7**, 7573–7582.

25. K. Miyazawa, Y. Kuwasaki, A. Obayashi and M. Kuwabara. *J. Mater. Res.* 2002, **17**, 83–88.

26. M. H. Nurmawati, P. K. Ajikumar, R. Renu, C. H. Sow and S. Valiyaveettil. *ACS Nano* 2008, **2**, 1429–1436.

27. M. Sathish, K. Miyazawa, J. P. Hill and K. Ariga. *J. Am. Chem. Soc.* 2009, **131**, 6372–6373.

28. C. Park, H. J. Song and H. C. Choi. *Chem. Commun.* 2009, 4803–4805.

29. D. Mi, H.-U. Kim, J.-H. Kim, F. Xu, S.-H. Jin and D. H. Hwang. *Synth. Met.* 2012, **162**, 483– 489.

30. H. Yu, H.-H. Cho, C.-H. Cho, K.-H. Kim, D. Y. Kim, B. J. Kim and J. H. Oh. *ACS Appl. Mater. Interfaces* 2013, **5**, 4865−4871.

31. Y. J. He, H.-Y. Chen, J. H. Hou and Y. F. Li. *J. Am. Chem. Soc.* 2010, **132**, 1377−1382.

32. C.-Z. Li, S.-C. Chien, H.-L. Yip, C.-C. Chueh, F.-C. Chen, Y. Matsuo, E. Nakamura and A. K. Y. Jen. *Chem. Commun.* 2011, **47**, 10082−10084.

33. K.-H. Kim, H. Kang, S. Y. Nam, J. Jung, P. S. Kim, C.-H. Cho, C. Lee, S. C. Yoon and B. J. Kim. *Chem. Mater.* 2011, **23**, 5090−5095.

34. I. Riedel, E. von Hauff, J. Parisi, N. Martin, F. Giacalone and V. Dyakonov. *Adv. Funct. Mater.* 2005, 15, 1979−1987.

35. N. Nakashima, T. Ishii, M. Shirakusa, T. Nakanishi, H. Murakami and T. Sagara. *Chem. Eur. J.* 2001, **7**, 1766–1772.

36. A. M. Cassell, C. L. Asplund and J. M. Tour. *Angew. Chem. Int. Ed.* 1999, **38**, 2403–2405.

37. J.-F. Nierengarten. *New J. Chem.* 2004, 28, 1177–1191.

38. X. Y. Meng, Q. Xu, W. Q. Zhang, Z. A. Tan, Y. F. Li, Z. X. Zhang, L. Jiang, C. Y. Shu and C. R. Wang. *ACS Appl. Mater. Interfaces* 2012, **4**, 5966−5973.

39. A. L. Rosa, K. Gillemot, E. Leary, C. Evangeli, M. T. González, S. Filippone, G. Rubio-Bollinger, N. Agraït, C. J. Lambert and N. Martín. *J. Org. Chem.* 2014, 79, 4871–4877.

40. X. Y. Meng, G. Y. Zhao, Q. Xu, Z. A. Tan, Z. X. Zhang, L. Jiang, C. Y. Shu, C. R. Wang and Y. F. Li. *Adv. Funct. Mater.* 2014, **24**, 158–163.

41. T. Homma, K. Harano, H. Isobe and E. Nakamura. *J. Am. Chem. Soc.* 2011, **133**, 6364–6370.

42. T. Nakanishi, W. Schmitt, T. Michinobu, D. G. Kurth and K. Ariga. *Chem. Commun.* 2005, 5982–5984.

43. T. Nakanishi, Y.-F. Shen, J.-B. Wang, H.-G. Li, P. Fernandes, K. Yoshida, S. Yagai, M. Takeuchi, K. Ariga, D. G. Kurth and H. Möhwald. *J. Mater. Chem.* 2010, **20**, 1253–1260.

44. T. Nakanishi, K. Ariga, T. Michinobu, K. Yoshida, H. Takahashi, T. Teranishi, H. Möhwald and D. G. Kurth. *Small* 2007, **3**, 2019–2023.

45. X. Zhang, T. Nakanishi, T. Ogawa, A. Saeki, S. Seki, Y. F. Shen, Y. Yamauchi and M. Takeuchi. *Chem. Commun.* 2010, **46**, 8752–8754.

46. X. Zhang, X. D. Li and L. X. Ma. *Chem. Res. Chin. Univ.* 2014, in press.

47. M. J. Frisch, G. W. Trucks, H. B. Schlegel, G. E. Scuseria, M. A. Robb, J. R. Cheeseman, G. Scalmani, V. Barone, B. Mennucci, G. A. Petersson, H. Nakatsuji, M. Caricato, X. Li, H. P. Hratchian, A. F. Izmaylov, J. Bloino, G. Zheng, J. L. Sonnenberg, M. Hada, M. Ehara, K. Toyota, R. Fukuda, J. Hasegawa, M. Ishida, T. Nakajima, Y. Honda, O. Kitao, H. Nakai, T. Vreven, J. A. Montgomery, Jr., J. E. Peralta, F. Ogliaro, M. Bearpark, J. J. Heyd, E. Brothers, K. N. Kudin, V. N. Staroverov, T. Keith, R. Kobayashi, J. Normand, K. Raghavachari, A. Rendell, J. C. Burant, S. S. Iyengar, J. Tomasi, M. Cossi, N. Rega, J. M. Millam, M. Klene, J. E. Knox, J. B. Cross, V. Bakken, C. Adamo, J. Jaramillo, R. Gomperts, R. E. Stratmann, O. Yazyev, A. J. Austin, R. Cammi, C. Pomelli, J. W. Ochterski, R. L. Martin, K. Morokuma, V. G.

Zakrzewski, G. A. Voth, P. Salvador, J. J. Dannenberg, S. Dapprich, A. D. Daniels, O. Farkas, J. B. Foresman, J. V. Ortiz, J. Cioslowski and D. J. Fox. *Gaussian 09, Revision C.01*, Gaussian, Inc., Wallingford CT, 2010.

48. M. Maggini, G. Scorrano and M. Prato. *J. Am. Chem. Soc.* 1993, **115**, 9798–9799.
49. H. Wang, Y. J. He, Y. F. Li and H. M. Su. *J. Phys. Chem. A* 2012, **116**, 255–262.
50. T. Suzuki, Y. Maruyama, T. Akasaka, W. Ando, K. Kobayashi and S. Nagasel. *J. Am. Chem. Soc.* 1994, **116**, 1359−1363.
51. M. Carano, T. D. Ros, M. Fanti, K. Kordatos, M. Marcaccio, F. Paolucci, M. Prato, S. Roffia and F. Zerbetto. *J. Am. Chem. Soc.* 2003, **125**, 7139−7144.
52. C. J. Brabec, A. Cravino, D. Meissner, N. S. Sariciftci, T. Fromherz, M. T. Rispens, L. Sanchez and J. C. Hummelen. *Adv. Funct. Mater.* 2001, **11**, 374−380.
53. M. C. Scharber, D. Mühlbacher, M. Koppe, P. Denk, C. Waldauf, A. J. Heeger and C. J. Brabec. *Adv. Mater.* 2006, **18**, 789−794.
54. F. B. Kooistra, J. Knol, F. Kastenberg, L. M. Popescu, W. Verhees, J. H. Kroon and J. M. Hummelen. *Org. Lett.* 2007, **9**, 551−554.
55. G. D. Han, W. R. Collins, T. L. Andrew, V. Bulović and T. M. Swager. *Adv. Funct. Mater.* 2013, **23**, 3061–3069.
56. X. Zhang and X. D. Li. *Chin. Chem. Lett.* 2014, **25**, 501–504.
57. The comparison of the HOMO and LUMO energies as well as energy gaps of C_{60} and PCBM calculated with various basis sets and experimental values were listed in Table S1 (ESI†). It showed that the PBEPBE/6-311G(d,p) basis set is more reliable than B3LYP/6-311G(d,p) for energy calculation based on geometry optimized with B3LYP/6-31G(d). Energies calculated from PBEPBE/6-311G(d,p) based on geometry optimized at the same level and at B3LYP/6-31G(d) level exhibited the comparable value but the former is more cost in computation time. Therefore, we selected the B3LYP/6-31G(d) level for geometry optimization but the PBEPBE/6-311G(d,p) for energy calculation by considering both reliability and computation cost.
58. S. S. Babu, A. Saeki, S. Seki, H. Möhwald and T. Nakanishi. *Phys. Chem. Chem. Phys.* 2011, **13**, 4830–4834.

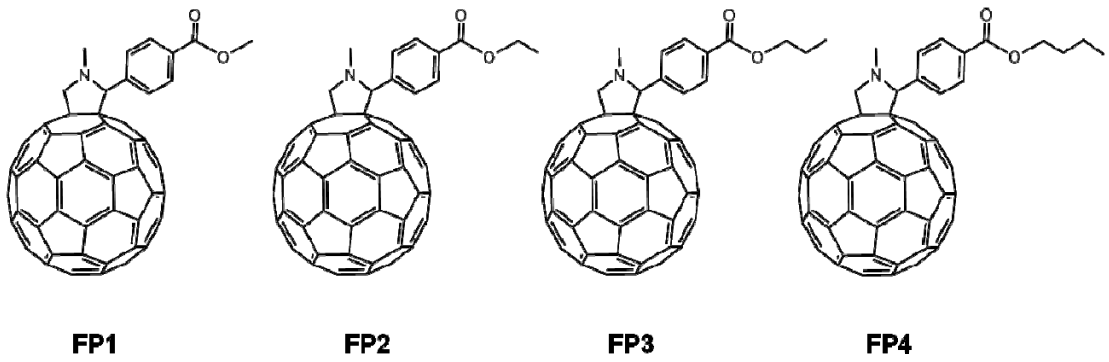

Scheme 1. Chemical structures of fulleropyrrolidine derivatives **FP1**–**FP4**.

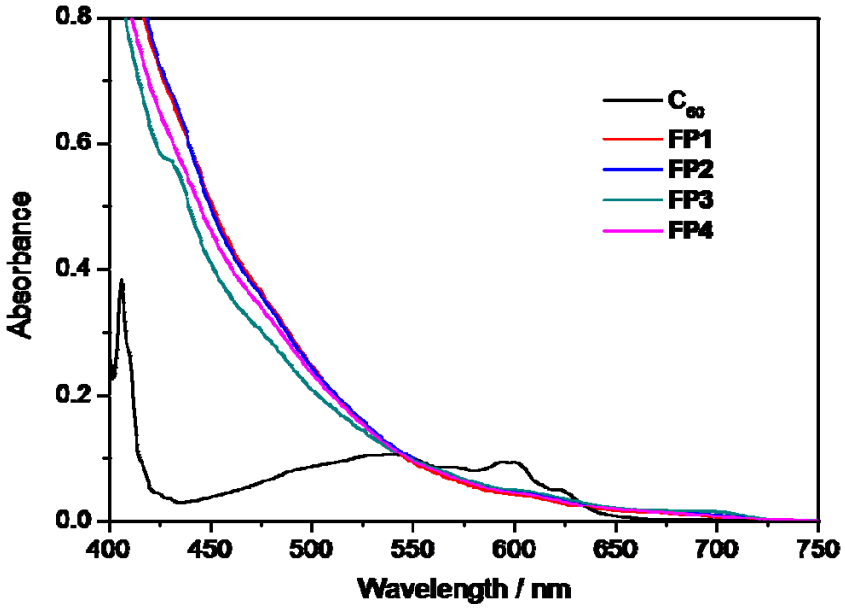

Figure 1. Absorption spectra of fulleropyrrolidines **FP1**–**FP4** and the pristine C_{60} in chloroform.

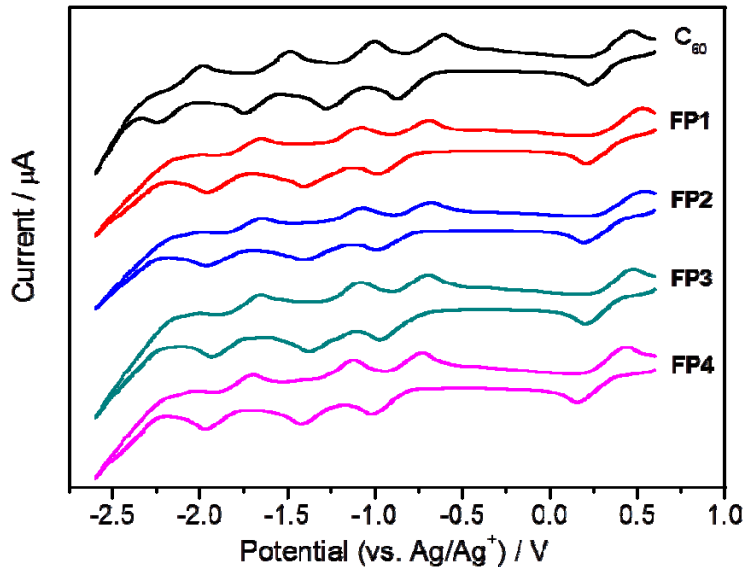

Figure 2. CV curves of fulleropyrrolidine derivatives **FP1**–**FP4** and the pristine C_{60} in o-DCB.

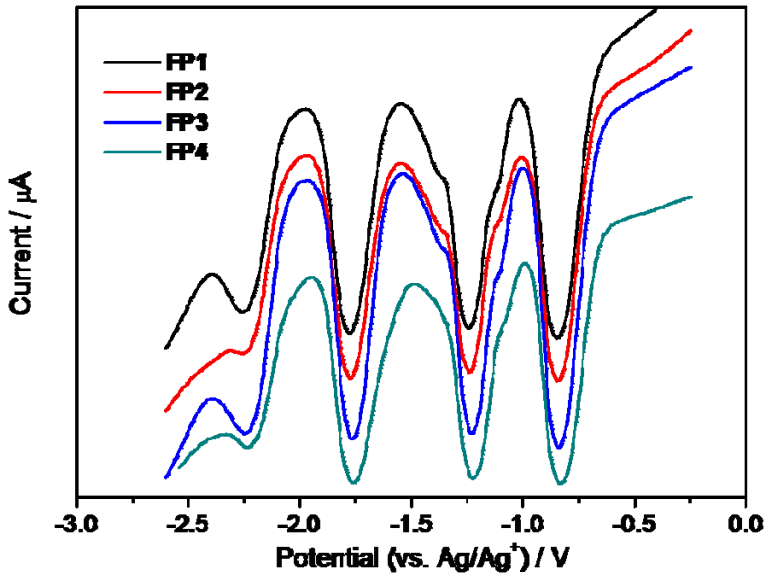

Figure 3. DPV curves of fulleropyrrolidine derivatives **FP1**–**FP4** in o-DCB. The parameters of DPV: amplitude, 0.05 V; pulse width, 0.2 s; sample width, 0.02 s; pulse period, 0.5 s.

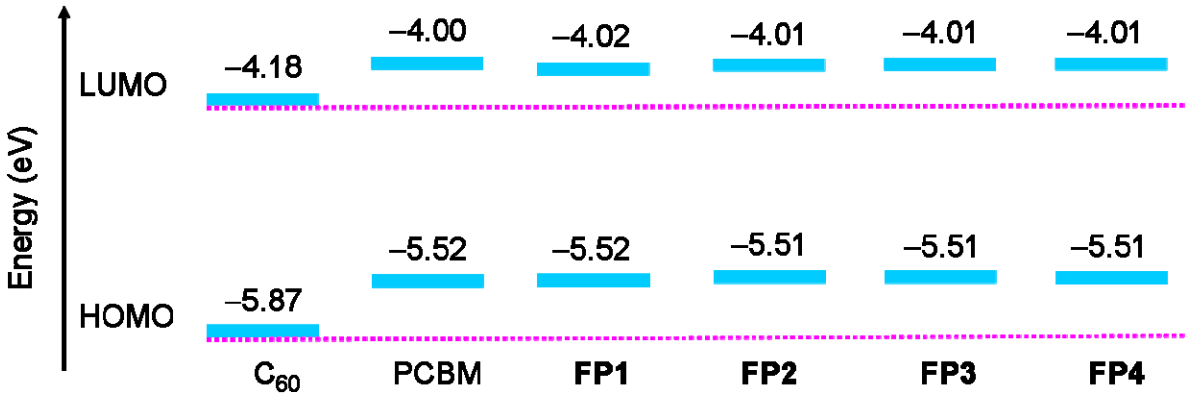

Figure 4. Schematic diagrams of HOMO and LUMO energy levels of C_{60}, PCBM, and fulleropyrrolidine derivatives **FP1**–**FP4** calculated at PBEPBE/6-311G(d, p) level.

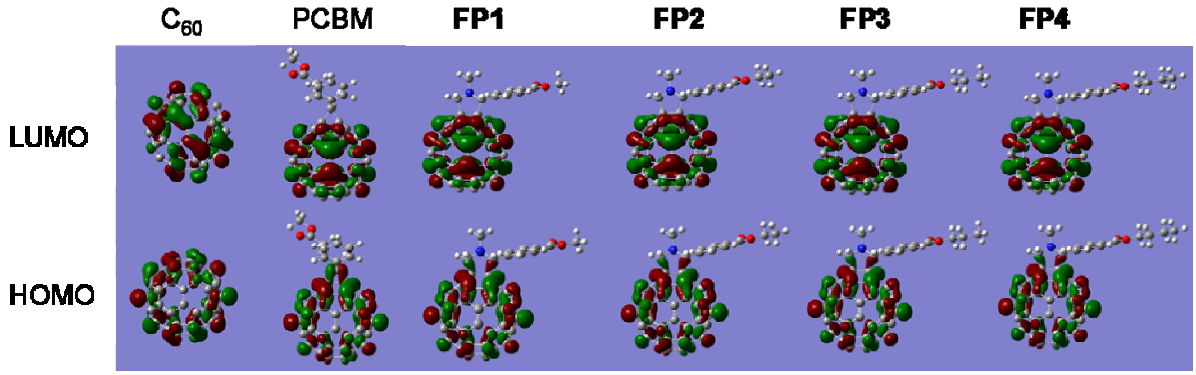

Figure 5. LUMO (top) and HOMO (bottom) contours for C_{60}, PCBM, and fulleropyrrolidine derivatives **FP1**–**FP4** calculated at PBEPBE/6-311G(d, p) level.

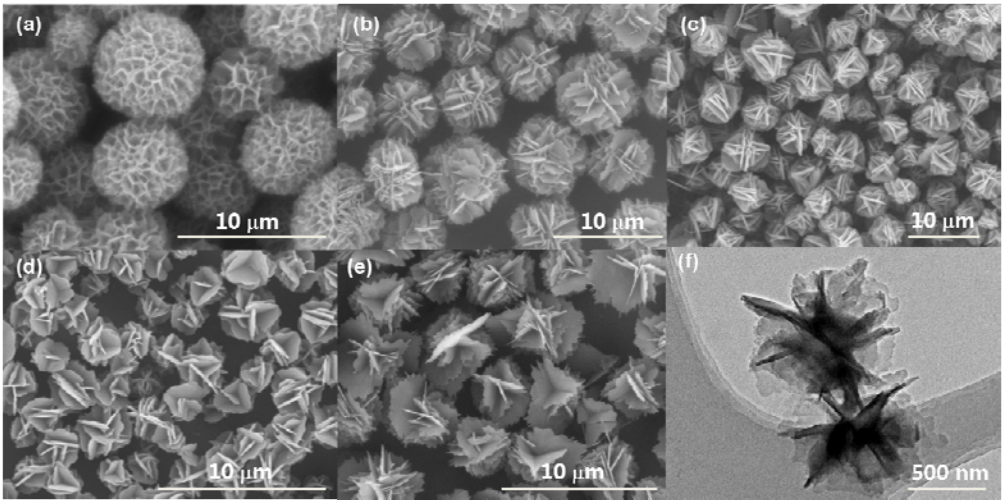

Figure 6. SEM (a-e) and TEM (f) images of self-organized architectures of **FP1**–**FP4** obtained from the mixture of chloroform/alcohol. (a) **FP1** from chloroform/2-propanol; (b) **FP2** from chloroform/2-propanol; (c) **FP3** from chloroform/2-propanol; (d) **FP4** from chloroform/ethanol; (e) and (f) **FP4** from chloroform/2-propanol.

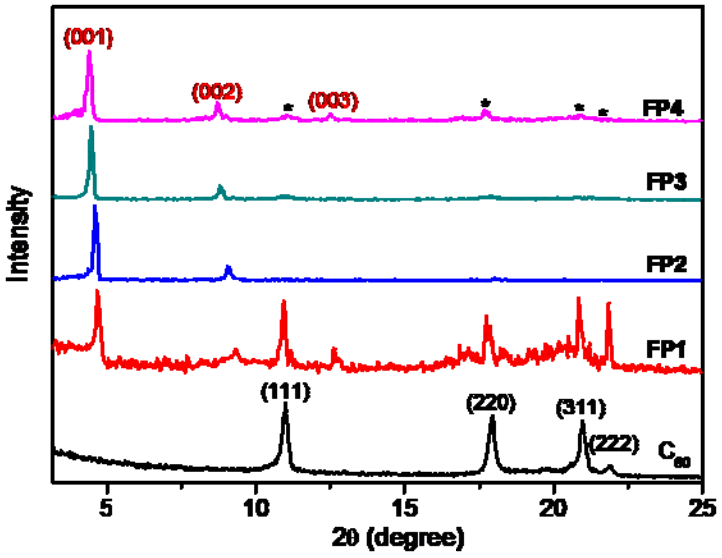

Figure 7. XRD patterns of flowerlike objects of **FP1**–**FP4** obtained from the mixture of chloroform/2-propanol.

Table 1 Redox properties, energy gaps, LUMO and HOMO energy levels of fullerenes **FP1**–**FP4**, PCBM and the pristine C_{60}.

Parameters	C_{60}	PCBM	**FP1**	**FP2**	**FP3**	**FP4**
E_1 [V][a]	–0.75	–0.90[h]	–0.84	–0.85	–0.85	–0.83
E_2 [V][a]	–1.14	–1.31[h]	–1.24	–1.24	–1.25	–1.23
E_3 [V][a]	–1.60	–1.85[h]	–1.77	–1.77	–1.78	–1.76
E_{onset}^{red} [V][b]	–0.68	–0.77[h]	–0.77	–0.78	–0.78	–0.78
LUMO [eV][c]	–3.92	–3.83	–3.83	–3.82	–3.82	–3.82
LUMO [eV][d]	–4.18	–4.00	–4.02	–4.01	–4.01	–4.01
λ_{onset} [nm][e]	693	723	724	724	724	724
E_{gap}[eV][f]	1.79	1.72	1.72	1.72	1.72	1.72
E_{gap}[eV][d]	1.69	1.52	1.50	1.50	1.50	1.50
HOMO [eV][g]	–5.71	–5.55	–5.55	–5.54	–5.54	–5.54
HOMO [eV][d]	–5.87	–5.52	–5.52	–5.51	–5.51	–5.51

[a] Half-wave potential. [b] Onset reduction potential. [c] LUMO = − e (E_{onset}^{red} + 4.60). [d] Values from the DFT calculation. [e] Onset absorption wavelength. [f] Band gap = hc/λ_{onset}, converted [J] to [eV]; h, Planks constant; c, speed of light. [g] HOMO = LUMO − E_{gap} [eV]. [h] Taken from ref. 55.